$Ba_{0.5}Sr_{0.5}Co_{0.8}Fe_{0.2}O_{3-\delta}$ Ceramic Hollow-Fiber Membranes for Oxygen Permeation

S. Liu
ARC Centre for Functional Nanomaterials, School of Engineering, The University of Queensland, Brisbane, Queensland 4072, Australia

X. Tan
Dept. of Chemical Engineering, Shandong University of Technology, Zibo 255049, China

Z. Shao
Key Laboratory of Materials-Oriented Chemical Engineering of Ministry of Education of China, College of Chemistry and Chemical Engineering, Nanjing University of Technology, Nanjing 210009, China

J. C. Diniz da Costa
ARC Centre for Functional Nanomaterials, School of Engineering, The University of Queensland, Brisbane, Queensland 4072, Australia

DOI 10.1002/aic.10966
Published online August 21, 2006 in Wiley InterScience (www.interscience.wiley.com).

Self-supported asymmetric hollow-fiber membranes of mixed oxygen-ionic and electronic conducting perovskite $Ba_{0.5}Sr_{0.5}Co_{0.8}Fe_{0.2}O_{3-\delta}$ (BSCF) were prepared by a combined phase-inversion and sintering technique. The starting inorganic powder was synthesized by combined EDTA–citrate complexing process followed by thermal treatment at 600°C. The powder was dispersed in a polymer solution and then extruded into hollow-fiber precursors through a spinneret. The fiber precursors were sintered at elevated temperatures to form gastight membranes, which were characterized by SEM and gas permeation tests. Performance of the hollow fibers in air separation was both experimentally and theoretically studied at various conditions. The results reveal that the oxygen permeation process was controlled by the slow oxygen surface exchange kinetics under the investigated conditions. The porous inner surface of the prepared perovskite hollow-fiber membranes considerably favored the oxygen permeation. The maximum oxygen flux measured was 0.031 $mol \cdot m^{-2} \cdot s^{-1}$ at 950°C with the sweep gas flow rate of 0.522 $mol \cdot m^{-2} \cdot s^{-1}$. To improve the oxygen flux of BSCF perovskite membranes, future work should be focused on surface modification rather than reduction of the membrane thickness. © 2006 American Institute of Chemical Engineers *AIChE J,* 52: 3452–3461, 2006
Keywords: air separation, mixed conducting ceramic, hollow-fiber membrane, perovskite membrane

Introduction

Some ceramics with defined structures such as perovskite and fluorite display mixed oxygen ionic and electronic conductivity at elevated temperatures. Exposed to oxygen partial pressure differential at high temperatures, the dense ceramic membranes derived from such materials are oxygen semipermeable without the need of external electrical loadings. The oxygen permselectivity is infinite, given that no species other than oxygen can be transferred through the membrane. These membranes have large potential and wide applications in the production of oxygen from air, selective oxidation of light hydro-

Correspondence concerning this article should be addressed to S. Liu at s.liu2@uq.edu.au.

carbons, oxygen-enriched combustion, coal gasification, decomposition of air pollutant NO to N_2, purification of metals from contaminations for iron and steel industry, and others, thus generating expanded research and development effort during the past two decades.[1-6]

Cales and Baumard first introduced the concept of using the mixed conducting solid oxides with a fluorite-type structure, such as $0.9ZrO_2$–$yCeO_2$–$0.1Y_2O_3$ with $0 < y < 0.9$, as oxygen semipermeable membranes.[7,8] From the perspective of application, membranes must possess sufficiently high oxygen permeability and good structural stability to withstand real process conditions (that is, light hydrocarbon reducing atmosphere, CO_2, and H_2O vapor). To address these problems, Teraoka et al.[9-11] developed high oxygen permeation flux membranes from $SrCo_{0.8}Fe_{0.2}O_3$ perovskite. The high permeation flux was attributed to the high concentration of oxygen vacancy in the lattice as a result of the total substitution of La^{3+} metal ion by Sr^{2+} in the A-site of perovskite. Although this material lacks sufficient chemical and structural stability in practical operation conditions, their breakthrough work encouraged the research community to explore new perovskite membranes with improved phase stability and oxygen permeability by optimizing the metal oxide composition in the ABO_3 perovskite structure. One example is the composition of $Ba_{0.5}Sr_{0.5}Co_{0.8}Fe_{0.2}O_{3-\delta}$ (BSCF), developed from $SrCo_{0.8}Fe_{0.2}O_{3-\delta}$ by partially substituted Sr with Ba of a larger ionic radius, which exhibits not only the highest oxygen permeation flux, but also favorable phase stability at high temperatures.[12]

In most previous studies in this area, disc-shaped membranes with only limited membrane area are usually used for oxygen permeation because they are easily prepared by the conventional static-pressing method. Although a multiple planar stack can be used to enlarge the membrane area to a plant scale, many engineering problems arise from flat designs such as sealing, connection, and pressure resistance. Tubular membranes have recently been developed to overcome these problems, although their small surface/volume ratios and the thick membrane walls make them unfavorable in practical applications. On the other hand, because of the symmetric structure of the disk or tubular membranes prepared, oxygen ion bulk diffusion is usually the rate-limiting step in air separation process resulting in a low oxygen permeation rate.

Alternatively, hollow-fiber membranes exhibit many advantages over planar and tubular membranes, such as higher surface area/volume ratio and facile high-temperature sealing. Although ceramic hollow-fiber membranes are still in their early stage of development, very important progress has recently been reported.[13-19] The well-established immersion-induced phase-inversion technique, commonly used to prepare polymeric hollow-fiber membranes, can be modified to prepare inorganic hollow-fiber precursors. Subsequently, the fiber precursors are heated to remove the polymer and sintered to a porous or dense structure. Compared to other methods, such as dry spinning[20] or wet spinning[21] a system of inorganic material and binder, depositing fibers from the gas phase to a substrate,[22] pyrolyzing the polymers,[23,24] etc., the combined phase-inversion and sintering technique is simple and requires no expensive equipment. More important, because the cross section of the hollow-fiber membranes prepared by phase inversion is asymmetric (that is, a thin dense layer integrated with a porous substrate),[25] the resistance to oxygen permeation is thus very low. As a result, hollow-fiber membranes have the potential to meet commercial targets in air separation units.

Table 1. Parameters for Preparing BSCF Hollow-Fiber Membranes and Gastightness of the Sintered Hollow Fibers

BSCF hollow-fiber spinning conditions	
Dope composition (wt %)	
BSCF precursor powder	70.6
PESf, Radel A-300	5.9
NMP	23.5
Dope temperature (°C)	23
Internal coagulant temperature (°C)	23
Injection rate of internal coagulant (mL/min)	20
Nitrogen pressure (psi)	40
Air gap (cm)	2
Linear extrusion speed (m/min)	2–7
Sintering time (h)	8
Gas permeance ($\times 10^8$) (mol m^{-2} Pa^{-1} s^{-1}) (He) of the sintered fibers	
Sintered at 950°C	314
Sintered at 1000°C	0.2
Sintered at 1050°C	0.05
Sintered at 1100–1190°C	0

In this study, BSCF hollow-fiber membranes (HFMs) were prepared by a combined phase-inversion spinning/sintering technique. The inorganic powder used as membrane material was synthesized by a modified Pechini technique. For a more in-depth understanding of BSCFHFM's performance in air separation, oxygen separation from air was carried out at various operating conditions.

Experimental

Preparation of BSCFHFMs

BSCF precursor powder used for membrane preparation was synthesized by a combined citrate and EDTA complexing method.[12] BSCF hollow-fiber membranes were prepared using a combined phase-inversion/sintering technique. The precursor powder was added to the polymer solution and the mixture was stirred for 24 h to ensure uniform distribution of the particles. The resulting suspension was subsequently degassed at room temperature and transferred to a stainless steel reservoir that was pressurized with nitrogen to 2.8×10^5 Pa. Extrusion was carried out through a tube-in-orifice spinneret with orifice diameter and inner diameter of 2.5 and 0.72 mm, respectively. The fibers emerging from the spinneret at 5 m/min were passed through an air gap of 2 cm and immersed in a water bath to complete gelation. Further detailed preparation procedures can also be found elsewhere.[15,17] The spinning conditions used in this study are shown in Table 1. The dried hollow fibers were heated in a furnace to 800°C at about 3°C/min and maintained at this temperature for 15 h to decompose and remove the polymer. Subsequent sintering was carried out at a temperature from 1000 to 1190°C for 8 h to obtain an impermeable structure. The fibers were finally cooled to room temperature at 2°C/min and tested for gastightness and air separation.

Gastightness of the hollow-fiber membranes

Hollow-fiber membranes were tested for gastightness using an apparatus shown schematically in Figure 1. The permeance of helium through the hollow fibers was measured at 2.03×10^5 Pa gas pressure difference across the membrane. One end

of the hollow fiber was sealed by the quick-setting epoxy resin, whereas the other end was left open. The He gas permeance was determined by the following equation:

$$P = \frac{Q}{A\Delta p} \tag{1a}$$

where P is the He permeance (mol/m^2·Pa·s), Q is the total He permeation rate (mol/s), A is the membrane area (m^2), and Δp is the partial pressure difference across the membrane (Pa). When the gas permeance is $<10^{-11}$ mol/m^2·Pa·s, it can be assumed to be gastight. The membrane area was calculated using Eq. 1b:

$$A = \frac{\pi L(D_o - D_i)}{\ln(D_o/D_i)} \tag{1b}$$

where D_o/D_i and L are, respectively, the outside/inside diameter of the hollow fiber (m) and the hollow-fiber length (m).

Oxygen Permeation Measurements

The experimental setup for oxygen permeation in the BSCF hollow-fiber membrane is shown in Figure 2a. BSCF fibers were connected on both sides with small-diameter quartz tubes and sealed with Ag paste. To conduct permeation measurements, the fiber with a length of 9 cm was placed into a tube furnace with the uniform heating length of 7 cm, thus two sealing sides occupy 2 cm length. The furnace was first heated to 950°C and maintained at this temperature for 60 min to soften the Ag and provide the required sealing. After cooling to 600°C and maintaining that temperature for 6 h to stabilize the membrane, the furnace was reheated to the measurement temperature. During measurement, an air flow of 300 mL/min was passed through a small quartz tube located in the furnace outside of the membrane to maintain constant air composition along the feed side of the fiber. The permeate gas was collected from the fiber lumen by He sweep gas and conducted to a GC (HP 5890II series) fitted with a washed molecular sieve 5Å column (6 ft × 1/8 in. × 0.085 in.; 80/100 mesh) for analysis. The flow rate was measured by an electronic flowmeter downstream of the fiber. The O_2 permeation flux was calculated by

$$J_{O_2} = \frac{C_{O_2}F}{A} \tag{2}$$

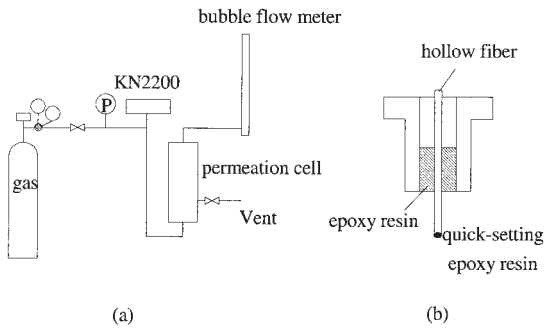

Figure 1. Apparatus for measuring gas permeation.

(a) Flow diagram, (b) permeation module.

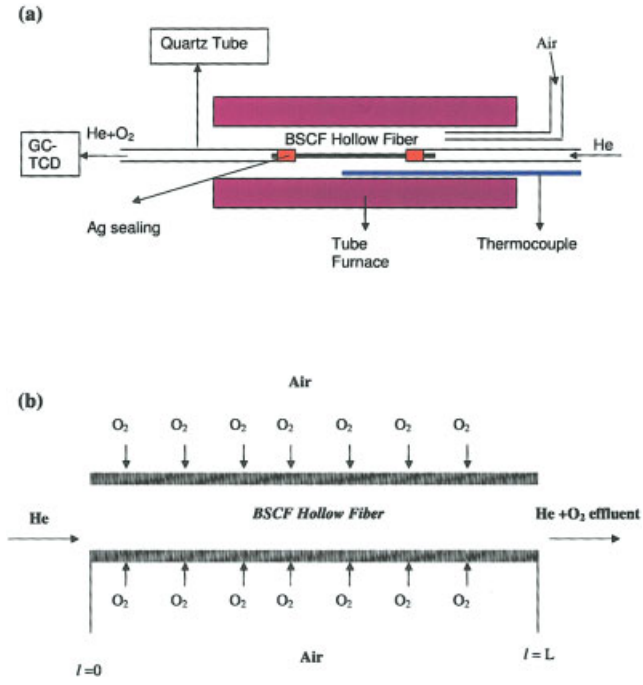

Figure 2. Permeation cell (a) and operating mode of BSCF hollow fiber for air separation (b).

[Color figure can be viewed in the online issue, which is available at www.interscience.wiley.com]

where J_{O_2} is the oxygen permeation flux (mol s^{-1} m^{-2}), C_{O_2} is the oxygen concentration (%), F is the flow rate of the permeate stream (mol/s), and A is the membrane area determined by Eq. 1b.

Model Development

Oxygen permeation through a mixed ionic-electronic conducting perovskite membrane from the high oxygen partial pressure side to the low oxygen partial pressure side includes the following steps in series:

(1) Mass transfer of gaseous oxygen from the gas stream to the membrane surface (high-pressure side).

(2) Surface reaction between the molecular oxygen and oxygen vacancies at the membrane surface (high-pressure side).

(3) Oxygen vacancy bulk diffusion across the membrane.

(4) Surface reaction between lattice oxygen and electron-hole at the membrane surface (low-pressure side).

(5) Mass transfer of oxygen from the membrane surface to the gas stream (low-pressure side).

Generally, the gas-phase resistance may be negligible compared to that of bulk diffusion and exchange reactions. As a result, the local oxygen permeation flux through a hollow-fiber (or tubular) membrane can be given by the following equation (the detailed derivation of which can be found elsewhere[26-28]):

$$\frac{dN_{O_2}}{dl} = \frac{k_r[(p'_{O_2})^{0.5} - (p''_{O_2})^{0.5}]}{\frac{(p''_{O_2})^{0.5}}{2\pi R_o} + \frac{k_f \ln(R_o/R_{in})(p'_{O_2})^{0.5}(p''_{O_2})^{0.5}}{\pi D_V} + \frac{(p'_{O_2})^{0.5}}{2\pi R_{in}}} \tag{3}$$

where N_{O_2} is the oxygen permeate molar flow rate in the fiber lumen (mol/s); l is the fiber length (m); p_{O_2} and p''_{O_2} are the oxygen partial pressures in the air and the lumen side, respectively (Pa); D_V is the diffusion coefficient of oxygen vacancy (m^2/s); and k_f and k_r are, respectively, the forward and the reverse reaction rate constants for the surface exchange reaction:

$$\frac{1}{2}O_2 + V''_O \overset{k_f/k_r}{\longleftrightarrow} O^x_O + 2h^{\bullet} \tag{4}$$

where O^x_O stands for lattice oxygen, $V^{\cdot\cdot}_O$ for oxygen vacancy, and $h^{\bullet}$ for electron hole.

When the membrane has a thickness far less than the critical thickness (L_c),[29] which is defined by the membrane thickness at which the oxygen permeation resistance by bulk diffusion equals that by the surface exchange reactions, the resistance by bulk diffusion can be negligible and the surface exchange reaction becomes the rate-limiting step. In this case, Eq. 3 can be simplified as

$$\frac{dN_{O_2}}{dl} = \frac{k_r[(p'_{O_2})^{0.5} - (p''_{O_2})^{0.5}]}{\frac{(p''_{O_2})^{0.5}}{2\pi R_o} + \frac{(p'_{O_2})^{0.5}}{2\pi R_{in}}} \tag{5}$$

In the formation of mathematical models, the following general assumptions were made:

(1) The mass transfer resistance of gas phase to oxygen permeation is negligible and the oxygen permeation process is controlled by the surface exchange reactions.

(2) Ideal gas law is applied to describe the gas behavior.

(3) The air composition along the fiber in the furnace tube is maintained constant.

(4) The gas stream in the fiber lumen is plug flow and the pressure drop is negligible.

(5) The operation runs at steady state.

Considering the above assumptions, Eq. 6 can be derived from Eq. 5:

$$\frac{d}{dl}\left(\frac{p''_{O_2}V}{RT}\right) = \frac{k_r[(0.21p_a)^{0.5} - (p''_{O_2})^{0.5}]}{\frac{(p''_{O_2})^{0.5}}{2\pi R_o} + \frac{(0.21p_a)^{0.5}}{2\pi R_{in}}} \tag{6}$$

where p_a is the atmosphere pressure in the furnace tube, V is the volumetric flow rate of the lumen stream, which can be related to the He flow rate, F_{He} by

$$\frac{(p_l - p''_{O_2})V}{RT} = F_{He} \tag{7}$$

with the boundary conditions

$$l = 0 \qquad p''_{O_2} = 0 \tag{8}$$

By substituting Eq. 7 into Eq. 6, it can be easily integrated numerically by the conventional Runge–Kutta method.

Results and Discussion

Membrane preparation and morphology study

Application of the immersion-induced phase-inversion technique to prepare inorganic hollow-fiber membranes seems versatile. Membranes can be produced from a wide selection of materials as long as the used inorganic powders and binder (polymer) solution are appropriate for making a spinning dope. In this work, the fine-grained inorganic powder (perovskite precursor) was prepared by the heat treatment of a dried intermediate resin synthesized by a combined citrate/EDTA complexing method at 600°C for 12 h. Figures 3a and 3b depict scanning electron microscopic (SEM) microphotographs of the extruded hollow-fiber precursors before heat treatment. The micrograph in Figure 3a illustrates that near the outer and inner walls of the fiber precursor, short finger-like structures are present. In addition, at the center (marked with red shape) of the hollow-fiber precursor, sponge-like structures are observed. The appearance of the fiber structures shown in Figure 3a can be attributed to the rapid precipitation that occurred at both the inner and outer fiber walls, resulting in finger-like voids and slow precipitation, giving the sponge-like structure at the center of the fiber. Figure 3b shows the outside surface of the hollow-fiber precursor before polymer removal. It is observed that most of these small particles (with a size of 1 micron) of inorganic powder are well dispersed and connected to each other by the polymer binder.

Figures 3c and 3d show the microstructure of the hollow fiber after relative mild heat treatment in air at a lower temperature of 800°C for 15 h to decompose the polymer and burn out the residual carbon. The cross-sectional structure of the sintered fiber as shown in Figure 3c has similarities with that of the precursor, that is, the sponge-like structures at the center are sandwiched by the short finger-like structures located at the outer and inner walls of the fiber. The microstructure of the external surface (Figure 3d) consists of uniform particles, unlike the structure of the fiber precursor shown in Figure 3b. At a heat treatment temperature of 800°C, there is little particle consolidation and particles are just weakly connected to each other, so the fiber mechanical strength is very low. Figure 3e is the X-ray diffraction (XRD) pattern of the crushed fibers after heat treatment. It is clearly shown that the majority of the fiber material is transformed to the perovskite phase, together with a small amount of $BaSO_4$, which is derived from a reaction between barium oxide and sulfur dioxide produced from the polyethersulfone (PESF) polymer in the oxygen-containing atmosphere.

Gastight membranes can be achieved by sintering at higher temperatures. The effects of the sintering temperature on the membrane properties and gas permeance are shown in Figure 4 and Table 1, respectively. BSCF grain growth with the increase of sintering temperature is clearly displayed by a comparison of Figures 4a–4d. Sintered at 1100°C, pores near the external surface of the hollow fibers are completely eliminated as a result of particle coalescence. Consequently, the resulting membrane became gastight, which was confirmed using a gas permeation test as shown in Table 1. It should be noted that the prepared gastight hollow-fiber membrane is not fully densified, although there is no connected porosity across the membrane. As shown in Figure 4f (a high-magnification cross-sectional SEM microphotograph), the asymmetric structure evolved

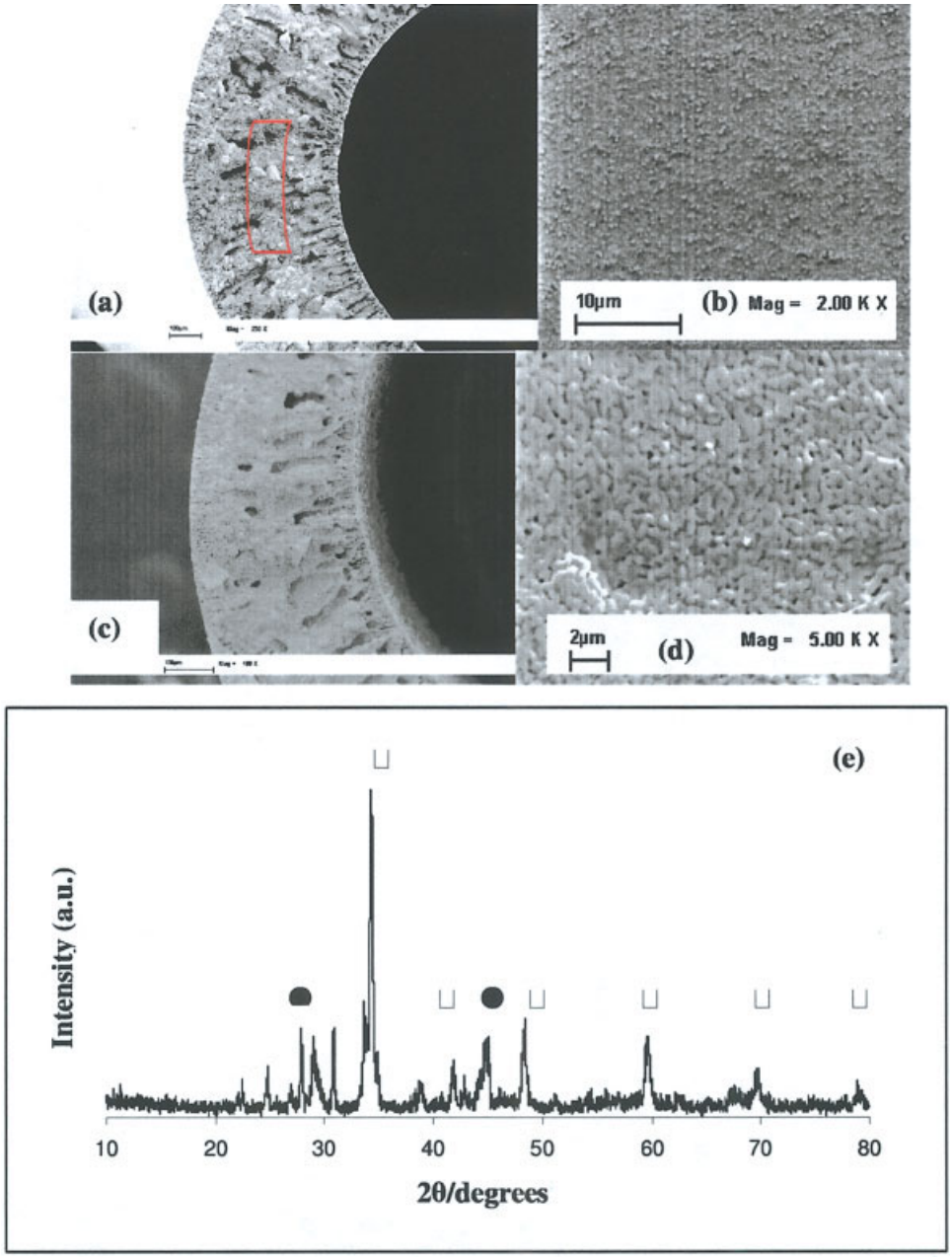

Figure 3. SEM microphotographs of the hollow fibers before (a: cross section; b: external surface) and after heat treatment (c: cross section; d: external surface) and XRD pattern (e) of the crushed sintered hollow fibers (● and ⊔ stand for the peaks of $BaSO_4$and BSCF perovskite, respectively).

[Color figure can be viewed in the online issue, which is available at www.interscience.wiley.com]

from the complex diffusion and phase-separation mechanisms is still well maintained. For example, the large finger-like pores (marked with red rings) are located near the center and smaller micron-sized pores are near the inside or outside surfaces (marked with red rectangles). To observe the surface interior structure, the skin layer of the fiber was peeled along the arrowhead direction displayed in Figure 4f. As shown in Figure 4g, the asymmetric layered honeycomb structure is clearly distinguishable. It can be seen that the thin dense layer is integrated onto the porous support of the same material. It should be noted that the fully densified layer should be near the outside surface because the inside surface of the hollow fiber is still porous (Figure 4h). However, at this stage, we are not sure after sintering, irrespective of whether the sponge-like layer at the center sandwiched by the porous structures is fully densified.

The thickness of the ion-conducting electrolyte layer should be made as thin as possible to maintain a low electrochemical resistance. To reduce the membrane thickness and at the same time retain the membrane mechanical strength, a conventional disk-shaped composite membrane structure is usually preferred. This process is expensive because it is accomplished by

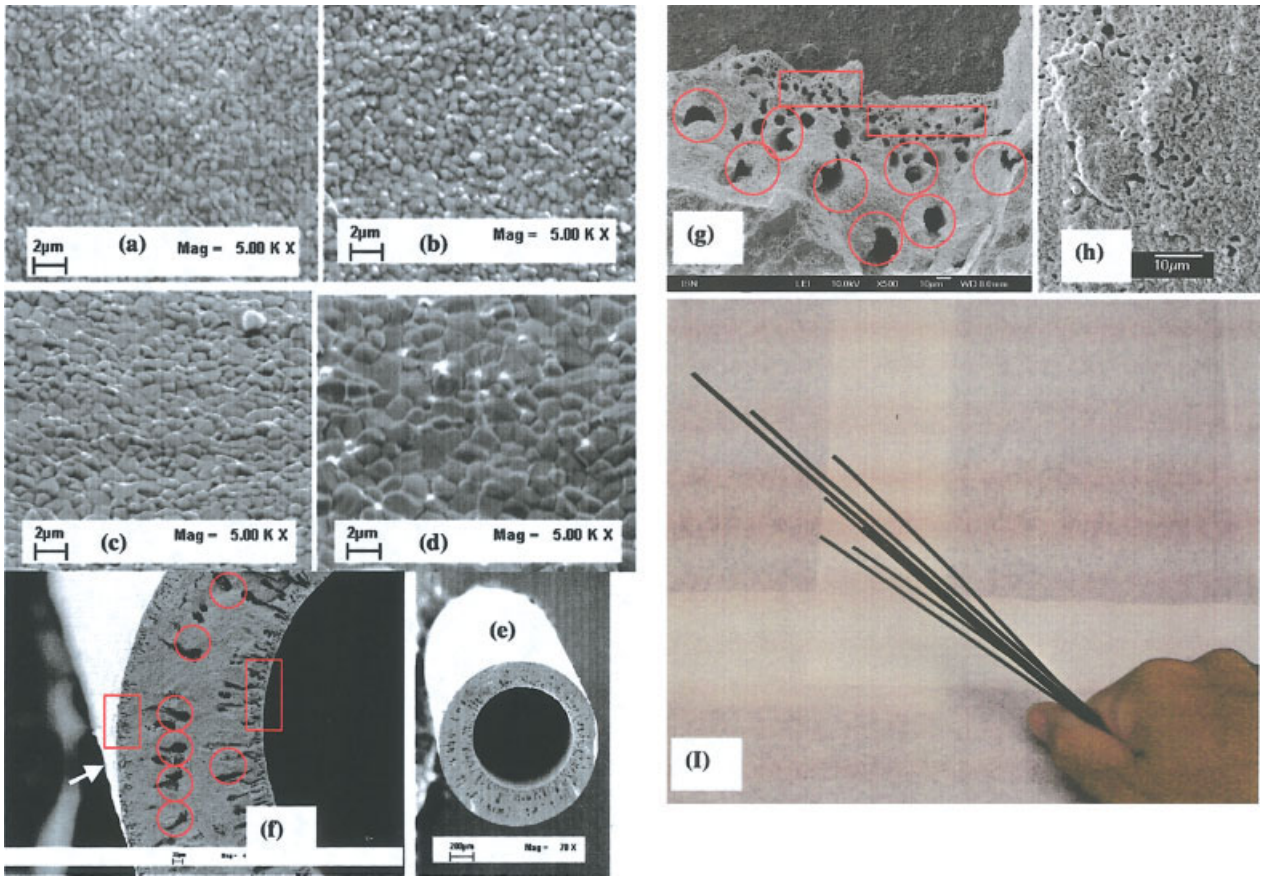

Figure 4. SEM microphotographs of the BSCFHFMs sintered at different temperatures [a: 950°C; b: 1000°C; c: 1050°C; d–h and I: 1100°C; a, b, c, and d: fiber external surfaces; e and f: cross section; g: layered honeycombed structure viewed from the arrowhead direction in f; h: fiber internal surface; and I: photograph of the prepared gastight BSCFHFMs].

[Color figure can be viewed in the online issue, which is available at www.interscience.wiley.com]

multiple fabrication steps. On the other hand, the prepared BSCFHFMs with asymmetric structure have four significant features compared to those of conventional disk-shaped membranes: (1) they are made from the same material, overcoming the problem of membrane deterioration arising from the mismatch of thermal expansion between two different materials used; (2) they are manufactured in a single step only using the immersion-induced phase-inversion technique, resulting in major savings in production time and costs; (3) the membrane is prepared in hollow-fiber geometry, providing the largest membrane area per unit volume ratio; and (4) the inner surface layer is porous and can provide more surface area for the oxygen exchange reaction. Figure 4I shows the photograph of the prepared gastight BSCFHFMs. Under our laboratory conditions, BSCFHFMs with OD 1.4 mm, thickness 0.20–0.5 mm, and length up to 30 cm can be fabricated by sintering at temperatures ranging from 1100 to 1190°C. It should be mentioned that because of the lower melting point, BSCF hollow fiber would melt to a shapeless mass if sintered at a temperature > 1200°C.

Oxygen permeation, modeling, and comparison with experimental data

Oxygen permeation was tested by oxygen extraction from air. As displayed in Figure 2, the outside surface of BSCFHFM was exposed directly to air and He as sweep gas was passed through the lumen. At high temperatures, oxygen will permeate from the air side to the lumen because of the oxygen concentration (or partial pressure) gradient across the membrane. Figure 5I shows the effect of operating temperature on the oxygen fluxes through three hollow fibers of A, B, and C prepared at 1000, 1100, and 1175°C, respectively, with dimensions given in Table 2. At He sweep flow rates around 0.23 $mol \cdot m^{-2} \cdot s^{-1}$, the temperature dependency of the oxygen permeation flux was investigated from 550 to 950°C. At temperatures < 600°C, the oxygen fluxes were very low and significant measurement error in excess of 100% could be observed. Appreciable high flux values were measured when the operating temperature was >700°C, which indicates that BSCF hollow fiber as oxygen-selective membranes can be used only at high temperatures. Above 700°C, the oxygen fluxes increased sharply with temperature as a result of the enhancement of oxygen diffusion or the oxygen surface reaction rates. For example, at the He sweep rate of 0.235 $mol \cdot m^{-2} \cdot s^{-1}$, the oxygen flux through the fiber sample B rose from 0.0033 to 0.020 $mol \cdot m^{-2} \cdot s^{-1}$ as the temperature increased from 750 to 950°C. Oxygen fluxes through other fibers show a similar growing trend with the change of operating temperature, but the flux through sample A is 20 to 50% higher than that

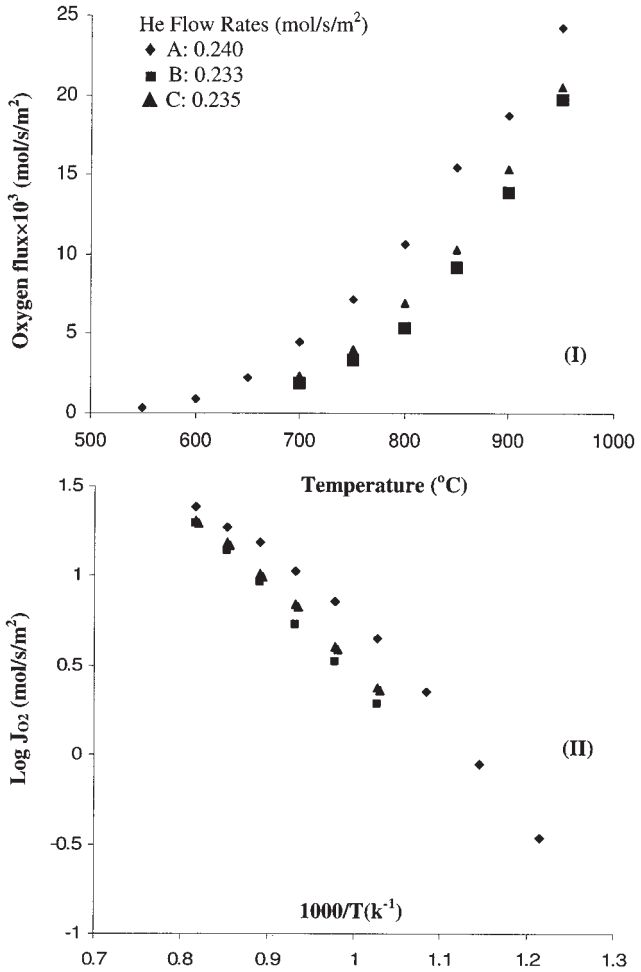

Figure 5. Effect of operating temperature on the oxygen fluxes through three fibers (I) and Arrhenius plot (II).

A, B, and C were prepared at 1000, 1100, and 1175°C, respectively.

obtained from fiber B or fiber C. Figure 5II shows Arrhenius plots of oxygen permeation fluxes through three hollow-fiber samples of A, B, and C. Applying the Arrhenius equation, activation energies for oxygen transport through fibers under the conditions of Figure 5 are 66.5 kJ/mol (fiber A) and about 90 kJ/mol (fibers B and C). Thus, fiber A had a lower activation energy, resulting in an enhanced oxygen permeation rate.

Oxygen permeation through a dense perovskite membrane can be controlled by the oxygen diffusion rate in the membrane as well as the surface oxygen exchange kinetics on either side of the membrane. For the purpose of clarifying controlling steps, the performance of four different BSCFHFMs with parameters shown in Table 2 in air separation was compared. It should be noted that the BSCFHFMs prepared at 1000°C are still thoroughly porous. According to the measured concentration of N_2, the leakage of oxygen through the pores or cracks was calculated and subtracted from the total oxygen flux according to a method described elsewhere.[15,17]

Figure 6 shows that the oxygen flux increased with the helium sweep rate, which is directly attributed to the lowering of oxygen pressure at the permeate side. For example, at 900°C, increasing the helium flow rate from 0.099 to 0.51 $mol \cdot m^{-2} \cdot s^{-1}$ will raise the oxygen flux through C from 0.011 to 0.018 $mol \cdot m^{-2} \cdot s^{-1}$. No saturation of oxygen flux was observed during the variation of the helium flow rates. Comparing all oxygen permeation fluxes, fiber A gave the best value, although fibers B and C exhibited a similar lower permeation rate. Figure 7 compares the oxygen fluxes through two fibers, which were sintered at the same temperature (1100°C) but have different fiber wall thickness. Again, fibers B and D displayed similar oxygen fluxes. Further comparing the fluxes of fibers B, C, and D, it was noted that the gastight BSCF hollow-fiber membranes prepared at different temperatures or with different thickness gave the same oxygen permeation rate at similar operating conditions (He sweep rate and temperature). These findings seem to suggest that the oxygen permeation process is controlled by surface oxygen exchange rate. To confirm this point, the oxygen transport was simulated using the models described above, which were developed on the assumption that surface reaction exchange is the rate-limiting step.

In Figures 6 and 7, oxygen fluxes (J_{O_2}) were used to characterize the oxygen permeation through the hollow-fiber membranes. It should be noted that oxygen fluxes calculated from Eq. 2 actually reflect the average oxygen permeation rates considering the whole membrane area. In fact, the real local oxygen permeation rate decreased along the fiber lumen direction because of the increase of oxygen concentration. In our theoretical simulation, O_2 concentration in the hollow-fiber exiting stream was predicted using the parameter as shown in Table 2. In addition, the simulated data were compared with the measured data as shown in Figures 6 and 7.

Figure 8 shows the theoretical values of oxygen concentration in the gas existing streams of the hollow fibers. For comparison purposes, the experimental data were also plotted in the same figure. As can be seen from Figure 8, at the same operating temperature, the O_2 concentration from the fiber permeate stream became lower as the sweep gas rate increased. However, for constant He sweep gas rate, more oxygen was extracted from air into the hollow fiber as the operating temperature increased, leading to higher oxygen concentration in

Table 2. Hollow-Fiber Samples Used for Oxygen Permeation Test and Theoretical Simulations

		Fiber Dimensions (mm)				Surface Reaction Exchange Rate (k_r)* [mol/(m²s)] × 10²		
Hollow Fiber Samples	Prep. Temp. (°C)	OD	ID	L	He Flow Rates (mol/s) × 10⁴	850°C	900°C	950°C
A	1000	1.47	0.97	70	0.11–1.34	2.1450	2.9124	4.2046
B	1100	1.33	0.83	70	0.13–1.33	1.3697	1.8984	3.1858
C	1175	1.41	0.99	70	0.10–1.11	1.3068	2.0746	3.2057
D	1100	1.40	1.0	72	0.12–1.32	1.2749	1.5669	3.0994

*k_r is obtained by model regression.

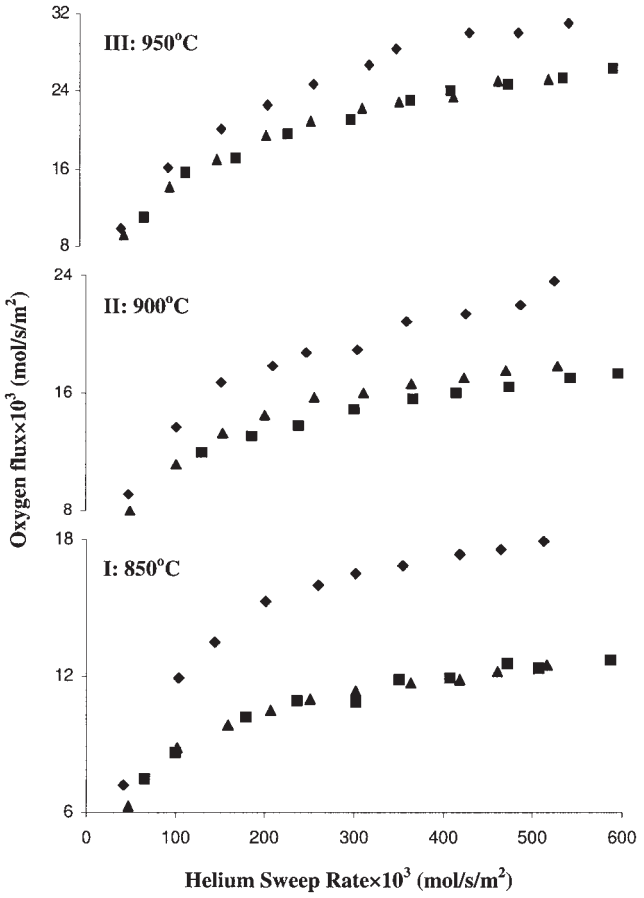

Figure 6. Effects of helium sweep rates on the oxygen fluxes through the fibers of Figure 5.

Fibers were prepared at A (◆): 1000°C; B (■): 1100°C; and C (▲): 1150°C, respectively.

the permeate gas streams. More important, the oxygen concentration from modeling results fitted very well with the experimental data for all samples examined. At this stage, these results strongly suggest that oxygen transport through the currently prepared BSCF hollow-fiber membranes is controlled by surface reaction exchange and this can be explained from membrane properties.

As discussed previously, the prepared gastight BSCF hollow-fiber membrane was of self-supported asymmetric layered honeycomb structure. Fibers B, C, and D were sintered at different temperatures or had different overall wall thickness, but the actual fully densified thickness of the BSCF layers (may be different) was far less than the critical thickness. Further, $Ba_{0.5}Sr_{0.5}Co_{0.8}Fe_{0.2}O_{3-\delta}$ (BSCF) displays higher oxygen ion conductivity than that of other perovskite membrane materials of $A_yA_{(1-y)}B_xB_{(1-x)}O_{(3-\alpha)}$, where A, A', B, and B' can be selected from La, Sr, Ca, Zr, Mg, Al, Ti, Cr, Mn, Fe, Co, Ni, Cu, Ga, Zr, or Zn. The thickness of the thin membrane, together with higher oxygen ion conductivity, made the bulk oxygen diffusion resistance very low and thus the oxygen transport was controlled by the slow surface oxygen exchange kinetics. Because of this, it is not difficult to understand that fibers B, C, and D resulted in similar oxygen permeation as reported in Figures 6 and 7. Compared to other fibers, fiber A was sintered at a much lower temperature (1000°C) and the membrane surface had a more porous structure, providing more surface area for oxygen exchange. Therefore, at similar operating conditions, the oxygen permeation rate of fiber A is higher than that of fibers B, C, and D. Recognition of the controlling step of the oxygen transport process will be of great help in developing or designing new membranes. For example, for the purpose of further improving oxygen permeation rate, it will be useful to modify the membrane surface by depositing a layer with higher oxygen permeation rate or a porous layer with

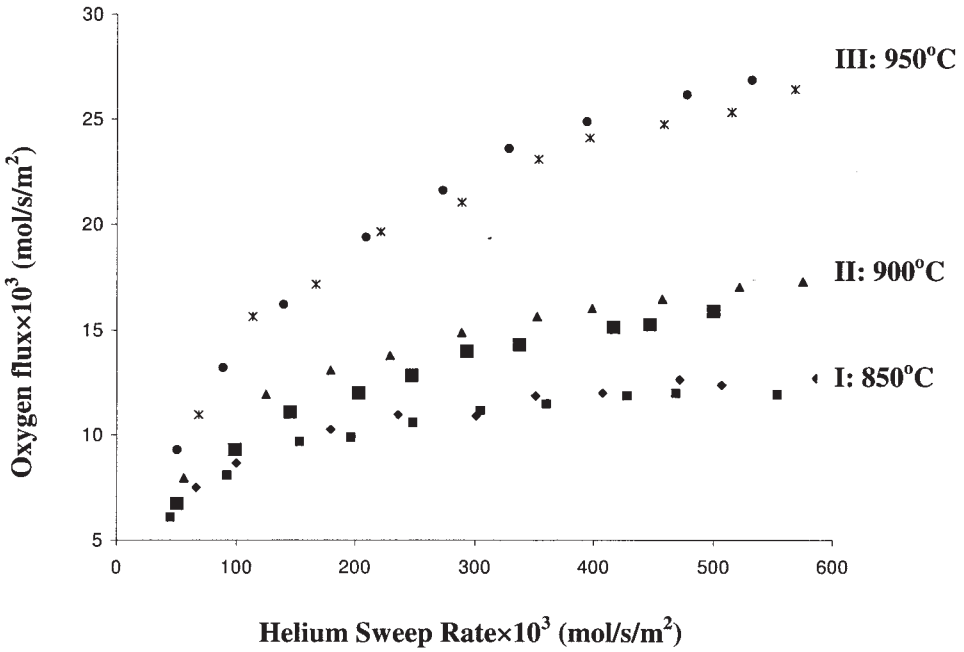

Figure 7. Effects of helium sweep rates and fiber wall thickness on the oxygen fluxes.

Fibers were prepared at 1100°C, with wall thickness of 0.25 mm (B: *, ▲, ◆) and 0.20 mm (D: small filled square, large filled square, ●).

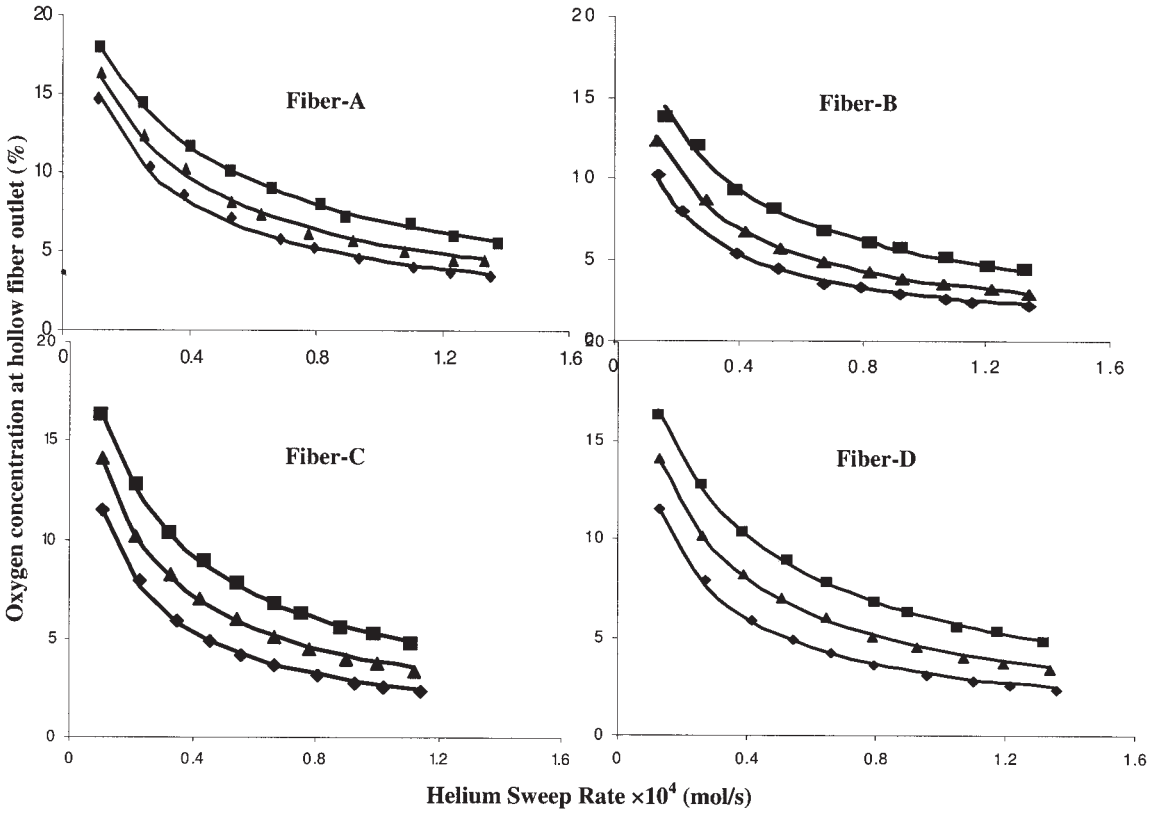

Figure 8. Comparison of oxygen concentration measurements with model predictions.

Measurement temperature: ◆: 850°C; ▲: 900°C; ■: 950°C. (Solid line: model).

higher surface area; however, it would be in vain to develop new BSCF hollow-fiber membranes with smaller wall thickness.

Conclusions

In summary, the gastight BSCF hollow-fiber membranes that possess an asymmetric honeycomb layered structure were prepared in a single-sintering step using an immersion-induced phase-inversion technique. The porous inner surface of the prepared BSCF hollow-fiber membranes is favorable for oxygen permeation. The maximum oxygen flux measured was 0.031 mol·m^{-2}·s^{-1} at 950°C with the sweep gas flow rate of 0.522 mol·m^{-2}·s^{-1}. The results from oxygen–air separation experiments and theoretical simulation indicate that the oxygen permeation process is controlled by the slow oxygen surface exchange rates.

Acknowledgments

The authors appreciate support from the ARC Centre for Functional Nanomaterials funded by the Australia Research Council under its Centre of Excellence Scheme. The authors also express sincere gratitude to Dr. Wang Rong in IESE (Singapore) for her insightful comments and valuable contributions toward completion of this article.

Notation

A = membrane area, m^2
C_{O_2} = oxygen concentration in argon effluent, %
D_V = effective diffusivity of oxygen vacancy, m^2/s
F = gas feed flow rate, mol/s
k_r = reverse surface reaction rate constant of Eq. 4, mol/(m^2·s)
k_f = forward surface reaction rate constant of Eq. 4, m/(Pa$^{0.5}$·s)
l = length variable of hollow-fiber membrane, m
L = length of hollow-fiber membrane, m
J_{O_2} = oxygen flux, mol/(m^2·s)
N_{O_2} = oxygen permeation molar flow rate, mol/s
P = gas permeance of membrane, mol/(m^2·s·Pa)
p_a = atmosphere pressure, 1.013×^{5}Pa
p_l = pressure in the fiber lumen, Pa
p_{O_2} = oxygen partial pressures in the shell side, Pa
p''_{O_2} = oxygen partial pressures in the lumen side, Pa
Δp = partial pressure difference, Pa
Q = permeation rate, mol/s
R = gas constant, 8.314 J/(mol·K)
R_{in} = inner radius of hollow fiber, m
R_o = outer radius of hollow fiber, m
T = operating temperature, K
V = volumetric flow rate of the lumen gas stream, m^3/s

Literature Cited

1. Dyer PN, Richards RE, Russek SL, Taylor DM. Ion transport membrane technology for oxygen separation and syngas production. *Solid State Ionics.* 2000;134:21-33.
2. Shao ZP, Dong H, Xiong GX, Gong Y, Yang WS. Performance of a mixed-conducting ceramic membrane reactor with high oxygen permeability for methane conversion. *J Membr Sci.* 2001;183:181-192.
3. Badwal SPS, Ciacchi FT. Ceramic membrane technologies for oxygen separation. *Adv Mater.* 2001;13:993-995.
4. Chen CS, Feng SJ, Ran S, Zhu DC, Liu W, Bouwmeester HJM. Conversion of methane to syngas by a membrane-based oxidation-reforming process. *Angew Chem Int Ed.*2003;42:5196-98.
5. Bouwmeester HJM. Dense ceramic membranes for methane conversion. *Catal Today.* 2003;82:141-150.
6. Wang H, Werth S, Schiestel T, Caro J. Perovskite hollow-fiber mem-

branes for the production of oxygen-enriched air. *Angew Chem Int Ed.* 2005;44:6906-6909.
7. Cales B, Baumard JF. Oxygen semipermeability and electronic conductivity in calcia-stabilized zirconia. *J Mater Sci.* 1982;17:3243-3248.
8. Cales B, Baumard JF. Mixed conduction and defect structure of ZrO_2-CeO_2-Y_2O_3 solid solutions. *J Electrochem Soc.* 1984;131:2407-2413.
9. Teraoka Y, Zhang H, Yamazone N. Oxygen-sorptive properties of defect perovskite-type $La_{1-x}Sr_xCo_{1-y}Fe_yO_{3-a}$. *Chem Lett.* 1985;1367-1370.
10. Teraoka Y, Zhang H, Furukawa S, Yamazone N. Oxygen-permeation through perovskite-type oxide. *Chem Lett.* 1985;1743-1746.
11. Teraoka Y, Zhang HM, Okamoto K, Yamazone N. Mixed ionic-electronic conductivity of $La_{1-x}Sr_xCo_{1-y}Fe_yO_{3-a}$. *Mater Res Bull.* 1988; 23:51-58.
12. Shao ZP, Yang WS, Cong Y, Dong H, Tong JH, Xiong GX. Investigation of the permeation behavior and stability of a $Ba_{0.5}Sr_{0.5}Co_{0.8}Fe_{0.2}O_3$ oxygen membrane. *J Membr Sci.* 2000;172:177-188.
13. Luyten J, Buekenhoudt A, Adriansens W, Cooymans J, Weyten H, Servaes F, Leysen R. Preparation of $LaSrCoFeO_{3-x}$ membranes. *Solid State Ionics.* 2000;135:637-642.
14. Liu S, Tan X, Li K, Hughes R. Preparation and characterisation of $SrCe_{0.95}Yb_{0.05}O_{2.975}$ hollow fibre membranes. *J Membr Sci.* 2001;193: 249-260.
15. Liu S, Gavalas GR. Oxygen selective ceramic hollow fiber membranes. *J Membr Sci.* 2005;246:103-108.
16. Tan X, Liu Y, Li K. Preparation of LSCF ceramic hollow fibre membranes for oxygen production by a phase-inversion/sintering technique. *Ind Eng Chem Res* 2006;45:142-149.
17. Liu S, Gavalas GR. Preparation of oxygen ion conducting ceramic hollow fiber membranes. *Ind Eng Chem Res.* 2005;44:7633-7637.
18. Schiestel T, Kilgus M, Peter S, Caspary KJ, Wang H, Caro J. Hollow fiber perovskite membranes for oxygen separation. *J Membr Sci.* 2005;258:1-4.
19. Wang H, Tablet C, Feldhoff A, Caro J. A cobalt-free oxygen-permeable membrane based on the perovskite-type oxide $Ba_{0.5}Sr_{0.5}Zn_{0.2}Fe_{0.8}O_3$. *Adv Mater.* 2005;7:1785-1788.
20. Smid J, Avci CG, Günay V, Terpstra RA, Van Eijk JPGM. Preparation and characterization of microporous ceramic hollow fibre membranes. *J Membr Sci.* 1996;112:85-90.
21. Lee KH, Kim YM. Asymmetric hollow inorganic membranes. *Key Eng Mater.* 1991;61/62:17-21.
22. Mineshige A, Inaba M, Ogumi Z, Takahashi T, Kawagoe T, Tasaka A, Kikuchi K. Preparation of yttria-stabilized zirconia microtube by electrochemical vapor-deposition. *J Am Ceram Soc.* 1995;78:3157-3159.
23. Koresh JE, Sofer A. Molecular-sieve carbon permselective membrane. 1. Presentation of a new device for gas-mixture separation. *Sep Sci Technol.* 1983;18:723-734.
24. Koresh JE, Sofer A. Mechanism of permeation through molecular-sieve carbon membrane. 1. The effect of adsorption and the dependence on pressure. *J Chem Soc Faraday Trans.* 1986;82:2057-2063.
25. Li K, Tan X, Liu Y. Single-step fabrication of ceramic hollow fibers for oxygen permeation. *J Membr Sci.* 2006;272:1-5.
26. Tan X, Li K. Modeling of air separation in a LSCF hollow-fiber membrane module. *AIChE J.* 2002;48:1469-1477.
27. Tan X, Liu Y, Li K. Mixed conducting ceramic hollow-fiber membranes for air separation. *AIChE J.* 2005;48:1991-2000.
28. Wang H, Wang R, Liang DT, Yang W. Experimental and modeling studies on $Ba_{0.5}Sr_{0.5}Co_{0.8}Fe_{0.2}O_{3-\delta}$ (BSCF) tubular membranes for air separation. *J Membr Sci.* 2004;243:405-415.
29. Bouwmeester HJM, Burggraaf AJ. Dense ceramic membranes for oxygen separation. In Gellings PJ, Bouwmeester HJM, eds. *The CRC Handbook of Solid State Electrochemistry.* Boca Raton, FL: CRC Press; 1997:481-500.

Manuscript received Apr. 17, 2006, and revision received Jun. 15, 2006.